

PARTICLE DETECTOR R&D

M.V.DANILOV

Institute for Theoretical and Experimental Physics, B.Chermushkinskaya 25, 117218

Moscow, RUSSIA

E-mail: danilov@itep.ru

Recent results on the particle detector R&D for new accelerators are reviewed. Different approaches for the muon systems, hadronic and electromagnetic calorimeters, particle identification devices, and central trackers are discussed. Main emphasis is made on the detectors for the International Linear Collider and Super B-factory. A detailed description of a novel photodetector, a so called Silicon Photomultiplier, and its applications in scintillator detectors is presented.

1 Introduction

Particle detector R&D is a very active field. Impressive results of the long term R&D for the Large Hadron Collider (LHC) are being summarized now by the four LHC detector collaborations. A worldwide effort is shifted to the detector development for the future International Linear Collider (ILC) and for the Super B-factory. The detector development for the FAIR facility has already started. Several groups perform R&D studies on detectors for the next generation of the hadron colliders.

This review is devoted mainly to the detector development for the ILC and Super B-factory. The vertex detectors are not discussed here in order to provide more details in other fields. R&D on the vertex detectors is very active and deserves a separate review. This review is organized following the radius of a typical collider detector from outside to inside.

2 Muon Detectors

Muon detectors cover very large areas. Therefore they should be robust and inexpensive. Resistive Plate Chambers (RPC) are often used in the present detectors, for example at the B-factories. In the streamer mode RPCs provide large signals. Hence it is possible to use very simple electronics. Another advantage is a possibility to have different

shapes of read out electrodes that match best the physics requirements. For example the BELLE RPCs have ring and sector shaped readout electrodes in the end cap regions.

The European CaPiRe Collaboration developed a reliable industrial technique for the glass RPC production¹. The production rate of more than 1000 square meters per day is possible. The RPC efficiency is larger than 95% up to the counting rates of $1Hz/cm^2$. This is reasonably adequate for the ILC detector but at the Super-B factory one expects by far larger rates. The RPCs in the proportional mode can stand about hundred times higher counting rates.

Scintillator strip detectors can work at even higher rates. A very attractive possibility is to use scintillator strips with Wave Length Shifting (WLS) fibers read out by so called Silicon Photo Multipliers (SiPM).

SiPM is a novel photo detector developed in Russia^{2,3,4}. It will be mentioned many times in this review. Therefore we shall discuss its properties in detail ^a. SiPM is a matrix of $1024 = 32 \times 32$ independent silicon photodiodes ^b covering the area of

^aThree groups developed such devices and produce them. They use different names for their products. We will use a generic name SiPM for all types of multipixel Si diodes working in the Geiger mode. New types of SiPMs are being developed by several groups including Hamamatsu

^bSiPMs can be produced with different number of pixels in the range 500-5000. We describe here the

$1 \times 1 \text{ mm}^2$. Each diode has its own quenching polysilicon resistor of the order of a few hundred $\text{k}\Omega$. All diode-resistor pairs, called pixels later on, are connected in parallel. A common reverse bias voltage V_{bias} is applied across them. Its magnitude of the order of $40 - 60 \text{ V}$ is high enough to start the Geiger discharge if any free charge carrier appears in the $p - n$ junction depletion region. The diode discharge current causes a voltage drop across the resistor. This reduces the voltage across the diode below the breakdown voltage $V_{breakdown}$ and the avalanche dies out. One diode signal is $Q_{pixel} = C_{pixel}(V_{bias} - V_{breakdown})$ where C_{pixel} is the pixel capacitance. Typically $C_{pixel} \sim 50 \text{ fF}$ and $\Delta V = V_{bias} - V_{breakdown} \sim 3 \text{ V}$ yielding $Q_{pixel} \sim 10^6$ electrons. Such an amplification is similar to the one of a typical photomultiplier and 3–4 orders of magnitude larger than the amplification of an Avalanche Photo Diode (APD) working in the proportional mode. Q_{pixel} does not depend on the number of primary carriers which start the Geiger discharge. Thus each diode detects the carriers created e.g. by a photon, a charged particle or by a thermal noise with the same response signal of $\sim 10^6$ electrons. Moreover the characteristics of different diodes inside the SiPM are also very similar. When fired, they produce approximately the same signals. This is illustrated in Fig. 1a. It shows the SiPM response spectrum when it is illuminated by weak flashes of a Light Emitting Diode (LED). First peak in this figure is the pedestal. The second one is the SiPM response when it detects exactly one photon. It is not known which diode inside the SiPM produces the signal since all of them are connected to the same output. However since the responses of all pixels are similar, the peak width is small. If several pixels in the SiPM are fired, the net charge signal is the sum of all charges. The third, fourth and so on peaks

in Fig. 1a correspond to 2, 3, ... fired pixels.

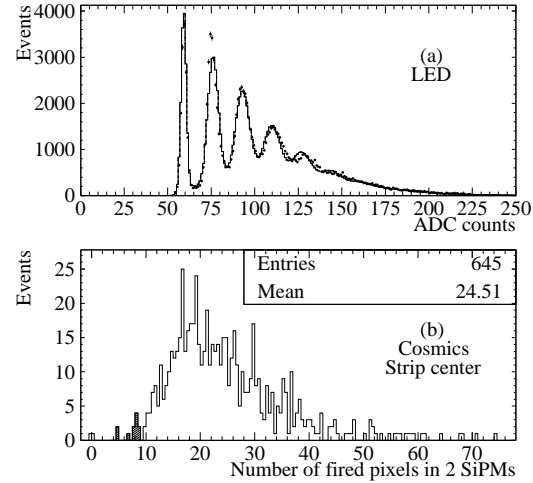


Figure 1. (a) SiPM response to short weak LED flashes. The fit curve is a simple model of the SiPM response. (b) Number of fired pixels in two SiPMs by a cosmic particle at the strip center. Few entries around zero belong to the pedestal.

The SiPM photodetection efficiency depends on the light wave length and the over-voltage ΔV . A typical value is about 10-15% for the green light. It includes geometrical inefficiency due to dead regions in the SiPM between the pixels. Thus SiPM and traditional photomultipliers have similar gain and efficiency. However, SiPM is approximately twice cheaper than one channel in the multianode photomultiplier and further cost reductions are expected in case of mass production. SiPM can work in the magnetic field, so there is no need in the light transportation out of the magnetic field. SiPM is so tiny that it can be mounted directly on the detector. This minimizes the light losses because of a shorter fiber length. SiPM has a quite high noise rate of about 2 MHz at 0.1 photoelectron threshold. However the noise rate drops fast with increasing threshold.

Fig. 1b shows the pulse height spectrum for cosmic particles obtained with the scintillator strip detector read out by two SiPMs ⁶.

SiPM used for the hadronic calorimeter prototype for the ILC⁵

The detector consists of a $200 \times 2.5 \times 1 \text{ cm}^3$ plastic scintillator strip and a wavelength shifting fiber read out by two SiPMs installed at the strip ends. The strip is extruded from the granulated polystyrene with two dyes at the “Uniplast” enterprise in Vladimir, Russia. The Kuraray multicladding WLS fiber Y11 (200) with 1 mm diameter is put in the 2.5 mm deep groove in the middle of the strip. No gluing is used to attach the WLS fiber to the SiPM or to the strip. There is about 200 μm air gap between the fiber end and the SiPM. To improve the light collection efficiency, the strip is wrapped in the Superradiant VN2000 foil produced by the 3M company.

In the worst case when the particle passes through the strip center there are 13.7 detected photons. The Minimum Ionizing Particle (MIP) signal in Fig. 1b is well separated from the pedestal. The detector efficiency averaged over the strip length is as high as $99.3 \pm 0.3\%$ at the 8 pixel threshold. Such a threshold is sufficient to reduce the SiPM noise rate to 5 kHz .

The ITEP group has also studied $100 \times 4 \times 1 \text{ cm}^3$ strips ⁷ with a SiPM ³ at one end of the WLS fiber and a 3M Superradiant foil mirror at the other end. The strips were produced by the extrusion technique in Kharkov. The strip surface was covered by a Ti oxide reflector co-extruded together with the strip. The Kuraray Y11, 1mm diameter fiber was glued into the 3mm deep groove with an optical glue. SiPM was also glued to the fiber. More than 13 photoelectrons per MIP were detected at the strip end far from the SiPM. With such a large number of photoelectrons the efficiency of more than 99% for MIP was obtained with the threshold of 7 photoelectrons. The detector can work at counting rates above 1 kHz/cm^2 . This is sufficient for the Super B-factory. Therefore the Belle Collaboration plans to use this technique for the K_L and muon system upgrade in the end cap region ⁸.

A scintillator tile structure can be used for even higher rates. Sixteen $10 \times 10 \times 1 \text{ cm}^3$ tiles read out by two SiPM ³ each were tested at the KEK B-factory ⁸. They demonstrated a stable performance adequate for the Super B-factory. An eight square meter cosmic test system for ALICE TOF RPC chambers is constructed at ITEP ⁹. It consists of $15 \times 15 \times 1 \text{ cm}^3$ tiles read out by two SiPMs ³ each. The counters have an intrinsic noise rate below 0.01 Hz , the time resolution of 1.2 nsec , and the rate capabilities up to 10 kHz/cm^2 .

3 Hadronic Calorimeters

The precision physics program at the future International Linear Collider (ILC) requires to reconstruct heavy bosons (W,Z,H) in hadronic final states in multijet events. In order to do this a jet energy resolution of better than $30\%/\sqrt{E}$ is required ¹⁰. The energy E is measured in GeV in this expression and in similar expressions for the energy resolution below. Monte Carlo (MC) simulations demonstrate that such a resolution can be achieved using a novel “particle flow” (PF) approach in which each particle in a jet is measured individually ¹¹. Momenta of charged particles are determined using tracker information. Photons are measured in the electromagnetic calorimeter (ECAL). Only neutrons and K_L should be measured in the Hadronic calorimeter (HCAL). They carry on average only about 12% of the jet energy. Therefore the HCAL can have modest energy resolution. The major problem is to reconstruct showers produced by charged tracks and to remove the corresponding energy from the calorimetric measurements. This requirement makes the pattern recognition ability to be a major optimization parameter of HCAL.

The CALICE Collaboration investigates two approaches for the HCAL. In the digital approach only one bit yes/no informa-

tion is recorded for each cell. Extremely high granularity of about $1\text{ cm}^2/\text{cell}$ is required in this case. In the analog approach the pulse height information is recorded for each cell. However a very high granularity of about $5 \times 5\text{ cm}^2/\text{cell}$ is still required¹². Such a granularity practically can not be achieved with a conventional readout approach with WLS fiber and a multianode photomultiplier (MAPM). The use of tiny SiPMs makes such a granularity achievable.

3.1 Analog Hadronic Calorimeters

A small 108 channel hadronic calorimeter prototype has been built in order to gain experience with this novel technique⁵. The calorimeter active modules have been made at ITEP and MEPhI. Scintillator tiles are made of a cheap Russian scintillator using a molding technique. A Kuraray Y11 1mm diameter double clad WLS fiber is inserted into a 2mm deep circular groove without gluing. The SiPM is placed directly on the tile and occupies less than 0.5% of a sensitive area. There is an air gap of about $100\mu\text{m}$ between the fiber and SiPM. Signals from SiPMs are sent directly to LeCroy 2249A ADCs via 25 meter long $50\ \Omega$ cables.

A lot of R&D has been performed in order to increase the light yield and the uniformity of the response. For better light collection the surface of the tiles is covered with 3M Superradiant foil. The tile edges are chemically treated in order to provide diffuse light reflection and separation between tiles. A light yield of more than 20 photoelectrons per MIP has been achieved for $5 \times 5 \times 0.5\text{ cm}^3$ tiles. Fig. 2 shows LED and β -source (^{90}Sr) signals from such a tile. Peaks with different number of photoelectrons are clearly seen. Signals from the β -source are very similar to MIP signals.

The HCAL prototype was successfully operated at the DESY electron test beam. Fig. 3 shows the linearity of the calorimeter

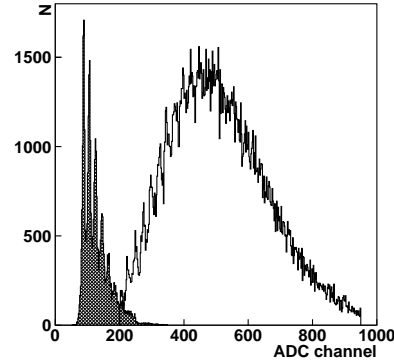


Figure 2. Pulse height spectrum from a tile with SiPM for low intensity LED light (hatched histogram) and for MIP signals from a β -source.

response measured with SiPM (circles) and MAPM (squares). The agreement between two measurements is better than 2%. The linear behavior of the SiPM result (better than 2%) demonstrates that the applied saturation correction due to limited number of pixels in the SiPM is reliable. The obtained energy resolution agrees well with MC expectations and with a resolution obtained using conventional MAPMs as well as APDs¹³. The obtained resolution of about $21\%/\sqrt{E}$ is modest since this is a hadron calorimeter.

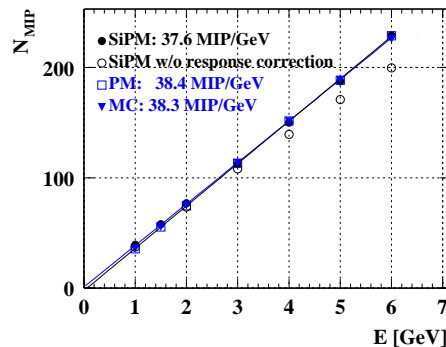


Figure 3. Calorimeter response normalized to number of MIPs versus beam energy; solid points (open circles) show SiPM data with (without) response function correction, squares are MAPM data and triangles are MC predictions.

The 8000 channel HCAL prototype with

the SiPM readout is being constructed by a subgroup of the CALICE Collaboration¹⁴. The $3 \times 3 \text{ cm}^2$ tiles are used in the central part of the calorimeter in order to test a semidigital approach. MC studies predict that the calorimeter with $3 \times 3 \text{ cm}^2$ cells and the 3 threshold measurement of the energy deposited in the tile should provide as good performance as a digital (yes/no) calorimeter with the $1 \times 1 \text{ cm}^2$ granularity¹⁵.

3.2 Digital Hadronic Calorimeters

The RPC based digital HCAL is developed by a subgroup of the CALICE collaboration¹⁶. They studied several RPC geometries and gases in order to optimize the efficiency and to reduce the cross-talk between pads. Fig. 4 shows the efficiency and pad multiplicity due to cross-talk obtained with the developed RPC prototype. The prototype consists of two sheets of floating glass with the resistive paint layer (1Mohm/square) and the gas gap of 1.2 mm. In works in the proportional mode and has the efficiency above 90% up to the rates of 50 Hz/cm^2 . The pad multiplicity is about 1.5. Much smaller pad multiplicity is observed in the RPC in which the readout electrode defines the gas sensitive volume instead of the glass sheet (see Fig. 4). It will be interesting to study further the properties of this promising RPC.

The GEM based digital HCAL is studied by another subgroup of the CALICE Collaboration¹⁷. They developed a procedure for the large area double GEM chamber production. A small prototype demonstrates the 95% efficiency at 40mV threshold and the pad multiplicity of 1.27. The 3M company plans to produce already in 2005 very long GEM foils of about 30 cm width.

The number of channels in the digital HCAL is enormous. Therefore cheap and reliable electronics is the key issue for this approach. The RPC and GEM digital HCAL teams develop jointly the electronics suitable

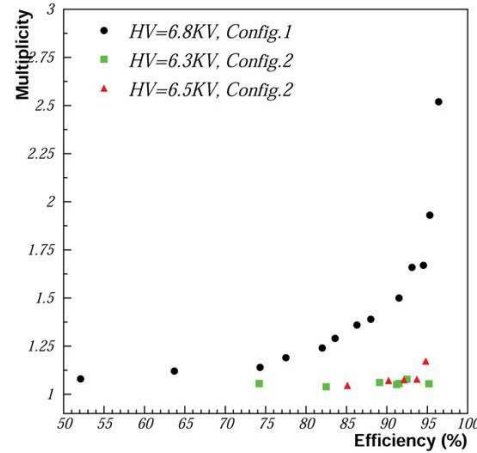


Figure 4. Pad multiplicity dependence on the efficiency for two types of RPC: full circles - standard RPC with two glass sheets; triangles and squares - the RPC with one glass sheet.

for both techniques.

3.3 The DREAM Calorimeter

Usually calorimeters have different response to electromagnetic and hadronic showers of the same energy. Therefore the fluctuations of the electromagnetic energy fraction in the hadron shower is one of the main reasons for the deterioration of the energy resolution.

In the Dual Readout Module (DREAM) calorimeter¹⁸ the electromagnetic energy in the hadronic shower is measured independently using quartz fibers sensitive only to the Cherenkov light produced dominantly by electrons. The visible energy is measured by scintillation fibers. The electromagnetic energy fraction in the shower can be determined by the comparison of the two measurements. This allows to correct for the different calorimeter response to the electromagnetic showers and to improve the energy resolution. A very similar response to electrons, hadrons, and jets was obtained in the DREAM calorimeter prototype after this correction. The ultimate energy resolution of the DREAM calorimeter is expected to be better than $30\%/\sqrt{E}$. Unfortunately the

shower leakage and insufficient amount of the Cherenkov light limited the measured prototype calorimeter resolution to $64\%/\sqrt{E}$ only.

The fluctuations of the visible energy because of the nuclear energy loss can be corrected for by adding to the DREAM structure the third type of fibers sensitive to neutrons. In this case the ultimate energy resolution of $15\%/\sqrt{E}$ is expected¹⁸. There are many nice ideas how to separate different mechanisms in the hadronic shower and to improve the energy resolution¹⁸. However they should be first demonstrated experimentally.

4 Electromagnetic Calorimeters

4.1 Electromagnetic Calorimeters for ILC

The requirement of a high granularity for the ILC detectors leads to the choice of very dense electromagnetic calorimeters with a small Mollier radius (R_M). Silicon/tungsten, scintillator/tungsten and scintillator/lead sandwich options are developed. The price for the high granularity is a modest energy resolution of the proposed calorimeters.

The CALICE collaboration constructs the Si/W prototype with about 10 thousand channels¹⁹. The pad size is as small as $1 \times 1 \text{ cm}^2$. The Si thickness is $500 \mu\text{m}$. The tungsten plate thickness is 1.4 mm , 2.8 mm , and 4.2 mm in the front, middle, and rare parts of the calorimeter. One third of the prototype has already been tested at the DESY electron beam and demonstrated a stable behavior. The signal to noise ratio of 8.5 was obtained for MIP. The tests of the whole calorimeter will start this Winter. The combined tests with the analog hadronic calorimeter are planned in 2006 as well.

The detector and readout plane thickness is 3.4 mm in the present prototype. It will be reduced to 1.75 mm including the readout chip in the final design resulting in $R_M = 1.4 \text{ cm}$.

The US groups (SLAC, UO, BNL) develop even more aggressive design of the Si/W calorimeter²⁰ for the small radius Si based ILC detector (ILC SiD). The detector and readout plane thickness is 1 mm only which results in the $R_M = 1.4 \text{ cm}$. Together with HPK they developed the Si detector consisting of 1024 hexagonal pads with 5 mm inner diameter. The detector is read out by a specially developed electronic chip²¹. The measured MIP signal in this detector is 26k electrons while the pedestal width is 780 electrons. The Si/W calorimeter for ILC is also developed in Korea²².

A hybrid scintillator/lead calorimeter prototype with three Si layers has been built and tested by the INFN groups²³. The $5 \times 5 \times 0.3 \text{ cm}^3$ scintillator tiles are combined into 4 longitudinal sections. Three layers of $9 \times 9 \text{ mm}^2$ Si pads are placed between the sections at 2, 6, and $12X_0$. The prototype demonstrated a good energy resolution of $11.1\%/\sqrt{E}$. It has the impressive spatial resolution of 2 mm at 30 GeV and e/π rejection below 10^{-3} . However it is not clear whether the granularity is sufficient for the PF method. Also the light transportation in the real detector will be extremely difficult. The use of SiPMs can solve the last problem.

The Japan-Korea-Russia Collaboration develops a scintillator/lead calorimeter with the SiPM readout²⁴. The active layer consists of two orthogonal planes of $200 \times 10 \times 2 \text{ mm}^3$ scintillator strips and a plane of $40 \times 40 \times 2 \text{ mm}^3$ tiles with WLS fibers. The fibers are readout by SiPMs developed at Dubna⁴. Even shorter strips of $40 \times 10 \times 2 \text{ mm}^3$ are considered as an alternative. The signal of 5p.e./MIP was obtained with the $200 \times 10 \times 2 \text{ mm}^3$ strips.

4.2 Electromagnetic Calorimeters for the Super B-Factory

Electromagnetic calorimeters for the Super B-factory should have a very good energy res-

olution and a fast response. They should be radiation hard up to about 10 kRad in the endcap region. The present CsI(Tl) calorimeters at the KEKB and SLAC B-factories can not stand the planned increase of the luminosity above $20ab^{-1}$. The CsI(Tl) light yield decreases to about 60% already at $10ab^{-1}$. There is also a large increase of PIN diode dark current. Finally the long decay time of about $1\mu sec$ leads to the pile up noise and fake clusters.

The BELLE Collaboration proposes to use pure CsI crystals with a phototetrode readout and a waveform analysis in the end cap region ²⁵. The shaping time is reduced from $1\mu sec$ to $30nsec$. The time resolution of better than $1nsec$ is achieved for energies above $25MeV$. The electronic noise is similar to the present CsI(Tl) calorimeters. The pure CsI crystals keep more than 90% of the light output after the irradiation of $7kRad$.

The BaBar Collaboration considers more radiation hard options of LSO or LYSO crystals and a liquid Xe calorimeter with the light readout ²⁶. The LSO and LYSO crystals are radiation hard, fast, and dense (see Table 1). They meet perfectly the requirements of the Super B-factory but their cost is prohibitively high at the moment. Liquid Xe is also an attractive option as it is seen in Table 1. The challenge here is the UV light collection. BaBar proposes to use WLS fibers and WLS cell coating for an immediate shift of the light wave length into a region with smaller absorption.

There is a good experience with very large liquid noble gas calorimeters. For example the $11m^3$ LiKr calorimeter at VEPP-4 has an excellent spatial ($\sim 1mm$) and energy ($\sim 3\%/\sqrt{E}$) resolution ²⁷.

4.3 The CMS Lead Tungstate Calorimeter

The CMS collaboration summarized at this conference their more than 10 year long R&D

Table 1. Properties of different scintillators.

Scintillator	CsI(Tl)	LSO	LiXe
Density (g/cc)	4.53	7.40	2.95
X_0 (cm)	1.85	1.14	2.87
R_M (cm)	3.8	2.3	5.7
λ scint.(nm)	550	420	175
τ scint.(ns)	680 3340	47	4.2, 22, 45
Photons/MeV	56k	27k	75k
Radiation hardness(Mrad)	0.01	100	-
cost(\$/cc)	3.2	~ 50	2.5

on the lead tungstate ($PbWO_4$) calorimeter ²⁸. The choice of $PbWO_4$ (Y/Nb) is driven by its small $X_0 = 0.89cm$, small $R_M = 2.19cm$, fast decay time of $\tau \sim 10nsec$, and a very high radiation hardness above $200kGy$. More than 37.000 crystal have already been produced at the Bogoroditsk (Russia). In spite of a small light yield of $\sim 8p.e./MeV$ the excellent energy resolution of 0.51% has been achieved at $120GeV$. Intensive R&D together with Hamamatsu resulted in excellent APD operated at a gain of 50. All 120.000 APDs passed a very strict acceptance test which included a $500krad$ irradiation and accelerated aging. Vacuum phototriodes (RIA, St.Petersburg) will be used in the endcaps because they are more radiation hard. The main challenge for CMS is to finish the production of crystals and to maintain the advantages of this approach in the big calorimeter.

5 Particle Identification

5.1 Cherenkov Counters

A novel type of proximity focusing RICH counter with a multiple refractive index (n)

aerogel radiator has been developed for the BELLE detector upgrade ²⁹. The multiple radiator allows to increase the radiator thickness and hence the Cherenkov photon yield without degradation in single photon angular resolution. With the refractive index of the consecutive layers suitably increasing in the downstream direction (focusing combination) one can achieve overlapping of Cherenkov rings from all layers (see Fig. 5). With the decreasing n (defocusing combination) one can obtain well separated rings from different layers (see Fig. 6).

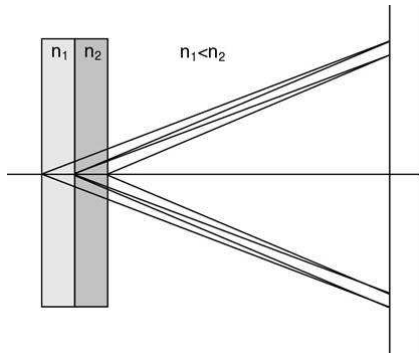


Figure 5. Principle of the dual radiator Ring Imaging Cherenkov counter .

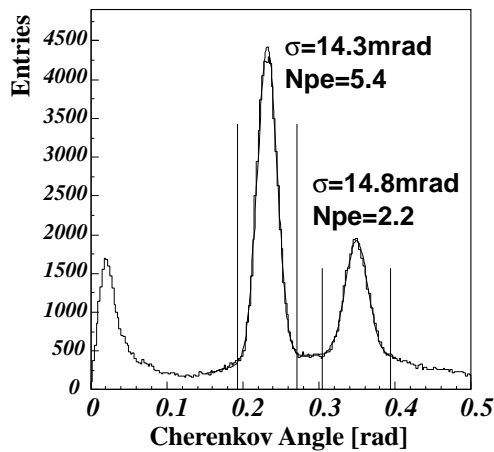


Figure 6. Distribution of the Cherenkov photon angles from 4GeV pions for a defocusing dual radiator with $n_1 = 1.057$ and $n_2 = 1.027$

Fig. 7 shows the performance of the detector with the single and multiple layer radiators. The number of detected photons is similar in two approaches but the single photon resolution is much better in the multiple layer configuration. The Cherenkov angle resolution of 4.5 $mrad$ per track was achieved with the triple layer radiator. This corresponds to the 5.1σ K/π separation at 4GeV.

The radiators with different refraction index layers attached directly at the molecular level have been produced at Novosibirsk ³⁰ and in Japan ²⁹.

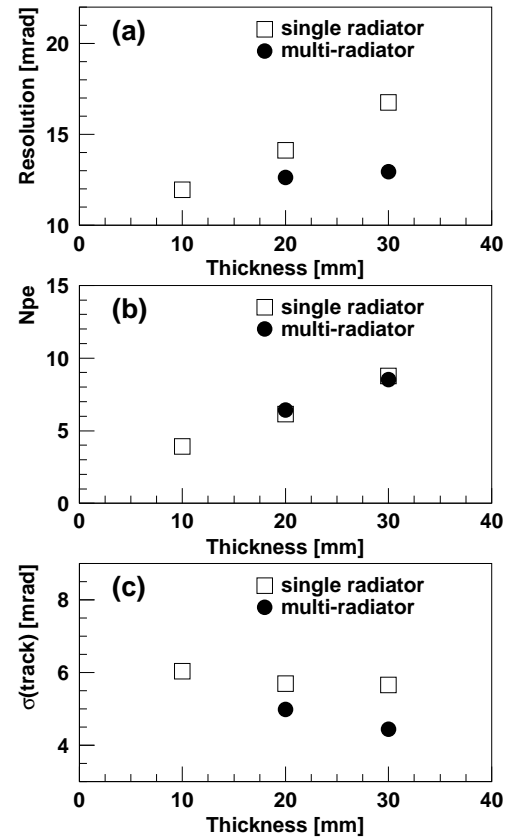


Figure 7. Single photon resolution (a), number of detected photons (b), and single track Cherenkov angle resolution for single and multiple focusing radiators for 4GeV pions.

The BaBar DIRC detector demonstrated an excellent performance. It is natural to consider the improved version of this tech-

nique for the Super B-factory. The SLAC and Cincinnati groups develop the Fast Focusing DIRC (FDIRC) detector ²⁶. The idea of this detector is illustrated in Fig. 8. With the accurate time measurement one gets a 3D image of the Cherenkov cone. In FDIRC the photon detection part is by far smaller than in DIRC. The development of the pixelated photodetectors with better than 100 nsec time resolution is a challenging task. The detail studies of Hamamatsu MAPM and Burley MCP PM at SLAC give very promising results. The FDIRC prototype is ready for tests at SLAC.

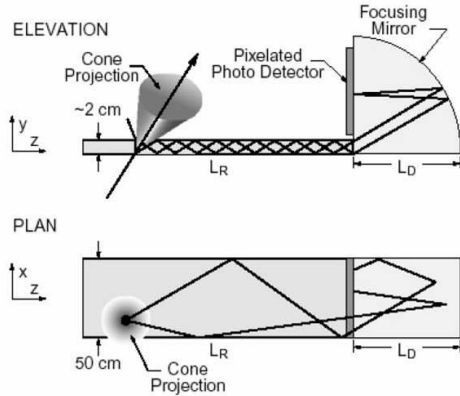


Figure 8. The principle of FDIRC operation.

In the Time of Propagation (TOP) counter the Cherenkov cone image is reconstructed from the coordinate at the quartz bar end and the TOP ³¹. The MCP PM SL10 is developed for TOP together with HPK. SL10 has 5 mm pitch and a single photon sensitivity in the 1.5T magnetic field. The time resolution of 30 psec has been achieved however the cross-talk is still a problem. The Ga/As photocathodes developed by HPK and Novosibirsk provide enough light for the $4\sigma\ \pi/K$ separation at 4 GeV . However the cathode life time is not sufficient yet. It loses 40% of quantum efficiency after collecting 350 mC/cm^2 which corresponds to 6 month operation at the Super B-factory.

5.2 TOF systems

A multilayer RPC (MRPC) with the excellent time resolution of better than 50 psec (see Fig.9) has been developed for the ALICE TOF system ³². It has the efficiency of about 99% at the counting rates as high as few hundred Hz/cm^2 . The MRPC has ten $220\ \mu\text{m}$ gaps. It would be interesting to investigate a possibility to use MRPC for K_L momentum measurements in the muon system at the Super B-factory.

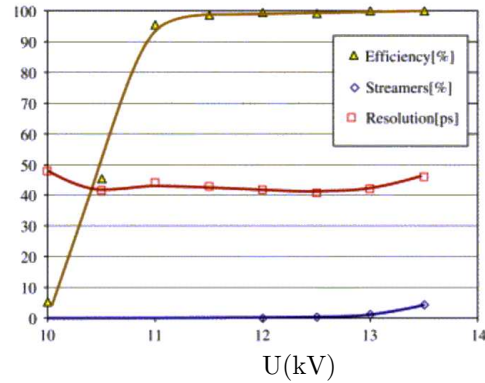


Figure 9. Efficiency (triangles, %), time resolution (squares, nsec), and streamer probability (circles, %) of MRPC versus applied voltage across 5 gaps (kV).

A time resolution of 48 psec was obtained with a $3 \times 3 \times 40\text{ mm}^3$ Bicron-418 scintillator read out directly by a $3 \times 3\text{ mm}^2$ SiPM without preamplifier ³³. The MIPs were crossing 40 mm in the scintillator. Therefore the signal was as big as 2700 pixels in the SiPM with 5625 pixels. The threshold was at 100 pixels. This approach is very promising for a super high granularity TOF capable to work in a very high intensity beams for example at FAIR.

6 Tracking

The Time Projection Chamber (TPC) is a natural choice for the ILC detector central tracker. This approach is developed by a large world wide collaboration ³⁴. TPC pro-

vides continues tracking through a large volume with a very small amount of material in front of the ECAL ($X_0 \sim 3\%$ in the barrel region). The dE/dx resolution of better than 5% helps in particle identification.

The thrust of the R&D is in the development of novel micro-pattern gas detectors which promise to have a better point and two track resolution than the traditional wire chambers. These detectors have smaller ion feedback into the TPC volume. Micromegas meshes and GEM foils are considered as main candidates. The spatial resolution of $\sim 100 \mu m$ was already achieved with GEM after the 65 cm drift in the 4 T field (see Fig. 10). Tests at smaller fields demonstrate that a similar resolution can be achieved with Micromegas as well. The double track resolution of $\sim 2 mm$ has been already demonstrated in small prototypes. By pitting a resistive foil above the readout pads it is possible to spread the signal over several pads. As a result the resolution improves up to the diffusion limit.

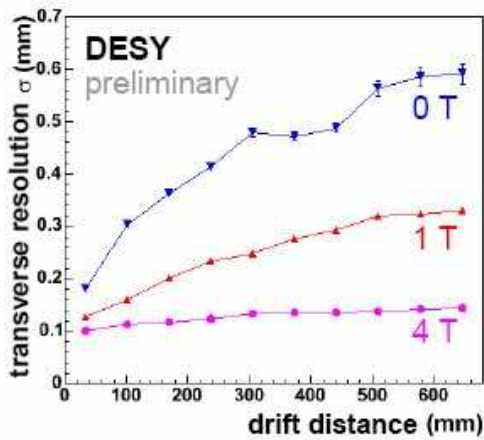


Figure 10. The transverse resolution dependence on the drift distance for three values of the magnetic field obtained in the TPC with a GEM readout.

A very exciting approach is a direct TPC readout with the MediPix2 chip ³⁴. This CMOS chip contains a square matrix of 256×256 pixels of $55 \times 55 \mu m^2$. Each pixel is

equipped with a low noise preamplifier, discriminator, threshold DAC and communication logic. The extremely high granularity allows to distinguish individual clusters in a track. Thus the ultimate spatial and dE/dx resolution can be achieved. Unfortunately the diffusion will severely limit both measurements. Nice tracks have been recorded by a prototype chamber equipped with Micromegas and MediPix2 (see Fig. 11). The number of observed clusters ($0.52/mm$ in a He/Isobutane 80/20 mixture) agrees within 15% with the expectations. The next step is to integrate the chip and Micromegas at the postprocessing step and to add the (drift) time measurement. Tracks were observed also with a GEM/MediPix2 prototype ³⁶. A

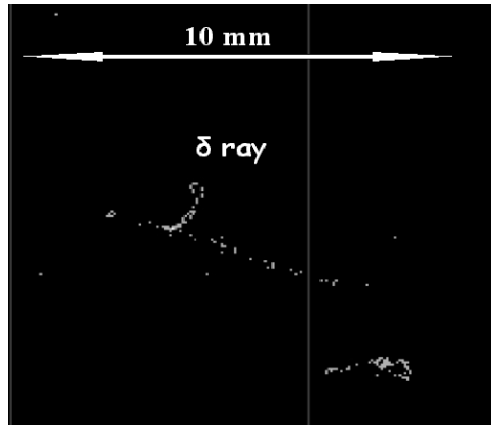


Figure 11. The transverse resolution dependence on the drift distance for three values of the magnetic field obtained in the TPC with a GEM readout.

compact all Si tracker is vigorously developed by the US groups ³⁵ for the small radius Si Detector for ILC. With small detector modules it is possible to reach a very good S/N ratio of about 20, to have a simple low risk assembly and relatively small amount of material of $\sim 0.8\% X_0$ per layer including a support structure. The pattern recognition is a serious issue for the Si tracker especially for tracks not coming from the main vertex.

The choice of the central tracker for the

Super B-factory depends crucially on the expected background which depends on the interaction region design.

In the BELLE study ²⁵ the background is expected to increase by a factor 20 from the present values. In this case the drift chamber with $13.3 \times 16 \text{ mm}^2$ cells is still adequate for the radius above 12.8 cm . Small $5.4 \times 5.0 \text{ mm}^2$ cells are foreseen for the radius between 10.2 cm and 11.6 cm .

In the BaBar study ³⁷ the luminosity term in the background extrapolation dominates. Therefore the background estimates are much higher than in the BELLE case. A drift chamber can not work in such environment. Therefore it is proposed to use the all Si tracker up to $R = 60 \text{ cm}$. A relatively large amount of material in the Si sensors and support structures leads to multiple scattering and considerable deterioration of the momentum and mass resolution. For example the mass resolution in the $B \rightarrow \pi^+ \pi^-$ decay mode deteriorates from 23 MeV in case of the drift chamber to 35 MeV in case of a conservative Si tracker design. Serious R&D efforts are required to make the Si tracker thinner. It should be also demonstrated that the pattern recognition in the Si tracker is good enough.

May be it is possible to develop an alternative solution to the Si tracker. Using the controlled etching the BINP-CERN group reduced the Cu thickness in GEM foils from 5 to $1 \mu\text{m}$ ³⁸. This allows to build the light triple GEM chamber with less than $0.15\% X_0$ including the readout electrode. The light double GEM chamber has even smaller thickness. The double and triple light GEM chambers were constructed and demonstrated identical performance with the standard GEM chambers. The light GEM chambers have a potential to provide the granularity and spatial resolution comparable to the Si tracker but with considerably smaller amount of material. However it is not clear so far how thick a support structure is needed. A lot of R&D studies are required to demon-

strate a feasibility of this approach.

7 Conclusions

The ongoing R&D should be sufficient to demonstrate the feasibility of detectors for the ILC and the Super B-factory. However there are many promising new ideas which have a potential to improve considerably the performance of the detectors and to exploit fully the physics potential of these colliders. The technologies for practically all detector subsystems are still to be selected on the basis of the R&D results. It is very important to strengthen and to focus the detector R&D especially for the ILC as it was done for the LHC collider.

8 Acknowledgments

This review would be impossible without many fruitful discussions with physicists working on the detector R&D for the LHC, ILC, and Super B-factory. In particular we are grateful to A. Bondar, J. Brau, B. Dolgoshein, J. Haba, E. Popova, F. Sefkow, R. Settles, A. Smirnitsky. This work was supported in part by the Russian grants SS551722.2003.2 and RFBR0402/17307a.

References

1. M. Piccolo, Proc. LCWS2005, SLAC (2004).
2. G. Bondarenko *et al.*, *Nucl. Phys. Proc. Suppl.* **61B** (1998) 347.
G. Bondarenko *et al.*, *Nucl. Instr. Meth.* **A442** (2000) 187.
P. Buzhan *et al.*, *ICFA Intstr.Bull.* **23** (2001) 28.
P. Buzhan *et al.*, *Nucl. Instr. Meth.* **A504** (2003) 48.
3. A. Akindinov *et al.*, *Nucl. Instr. Meth.* **A387** (1997) 231.
4. Z. Sadygov *et al.*, arXiv:hep-ex/9909017 and references therein.

5. V. Andreev *et al.*, *Nucl. Instr. Meth.* **A540** (2005) 368.
6. V. Balagura *et al.* Paper 241 contributed to this Symposium. V. Balagura *et al.* arXiv: Physics/0504194.
7. V. Balagura *et al.*, To be published in *Nucl. Instr. Meth.*.
8. M. Danilov, Talk at the 6th Workshop on Higher Luminosity B-Factory, KEK (2004), <http://belle.kek.jp/superb/workshop/2004/HL6/>.
9. A. Akindinov *et al.*, Submitted to *Nucl. Instr. Meth.*.
10. See e.g. F. Sefkow, Proc. Calor2004, Perugia (2004).
11. V. Morgunov, Proc. Calor2002, CALTECH (2002). H. Videau and J. C. Brient, Proc. Calor2002, CALTECH (2002).
12. M. Danilov, Proc. LCWS04, Paris (2004).
13. V. Andreev *et al.*, To be published in *Nucl. Instr. Meth.*.
14. F. Sefkow, Proc. LCWS2005, SLAC (2005), <http://www-conf.slac.stanford.edu/lcws05/>.
15. V. Zutshi, Proc. LCWS04, Paris (2004).
16. J. Repond, Proc. LCWS05, SLAC (2005).
17. A. White, Proc. LCWS05, SLAC (2005).
18. R. Wigmans, Proc. LCWS05, SLAC (2005).
19. J-C. Brient, Proc. LCWS05, SLAC (2005).
20. D. Strom, Proc. LCWS05, SLAC (2005).
21. M. Breidenbach, Proc. LCWS05, SLAC (2005).
22. S. Nam, Proc. LCWS05, SLAC (2005).
23. P. Checchia, Proc. LCWS05, SLAC (2005).
24. D. H. Kim, Proc. LCWS05, SLAC (2005).
25. K. Abe *et al.* SuperKEKB LoI, KEK Report 04-4 (2004).
26. D. Hitlin, Talk at the Super B-Factory Workshop, Hawaii (2004) <http://www.phys.hawaii.edu/superb04/>.
27. V. A. Aulchenko *et al.*, *Nucl. Instr. Meth.* **A419** (1998)602; Yu. Tikhonov, Private communication.
28. M. Lethuillier (CMS), Paper 131 contributed to this Symposium.
29. T. Iijima *et al.*, arXiv: Physics/0504220.
30. A. Yu. Barnyakov *et al.*, Proc. RICH2005, to be published in *Nucl. Instr. Meth.*.
31. K. Inami, Talk at the Super B-Factory Workshop, Hawaii (2004).
32. A. Akindinov *et al.*, *Nucl. Instr. Meth.* **A456**(2000) 16.
33. A. Karakash, Talk at the 4th Conference on New Developments in Photodetection Beaune (2005).
34. R. Settles, Paper 222 contributed to this Symposium.
35. T. Nelson, Proc. LCWS05, SLAC (2005).
36. M. Titov, Private communication; Paper submitted to IEEE Nuclear Science symposium, Puerto Rico (2005).
37. G. Calderini, Talk at the Super B-Factory Workshop, Hawaii (2004).
38. A. Bondar, Private communication.